Bioprocess and Biosystems Engineering (2023) 46:89–103
https://doi.org/10.1007/s00449-022-02815-8

RESEARCH PAPER

# In vitro anticancer and antibacterial performance of biosynthesized Ag and Ce co-doped ZnO NPs

**Nouf M. Al-Enazi[1] · Khawla Alsamhary[1] · Mansour Kha[2] · Fuad Ameen[3]**

Received: 17 August 2022 / Accepted: 14 November 2022 / Published online: 20 December 2022


## Abstract

The great potential of zinc oxide nanoparticles (ZnO NPs) for biomedical applications is attributed to their physicochemical properties. In this work, pure and Ag and Ce dual-doped ZnO NPs were synthesized through a facile and green route to examine their cytotoxicity in breast cancer and normal cells. The initial preparation of dual-doped nanoparticles was completed by the usage of *taranjabin*. The synthesis of Ag and Ce dual-doped ZnO NPs was started with preparing the Ce:Ag ratios of 1:1, 1:2, and 1:4. The cytotoxicity effects of synthesized nanoparticles against breast normal cells (MCF-10A) and breast cancer cells (MDA-MB-231) were examined. The hexagonal structure of synthesized nanoparticles was observed through the results of X-ray diffraction (XRD). Scanning electron microscopy (SEM) images exhibited the spherical shape and smooth surfaces of prepared particles along with the homogeneous distribution of Ag and Ce in ZnO with high-quality lattice fringes without any distortions. According to the cytotoxic results, the effects of Ag/Ce dual-doped ZnO NPs on breast cancer (MDA-MB-231) cells were significantly more than of pure ZnO NPs, while dual-doped and pure nanoparticles remained indifferent towards breast normal (MCF-10A) cells. In addition, we investigated the antimicrobial activity against harmful bacteria.

✉ Nouf M. Al-Enazi
n.alenazi@psau.edu.sa

[1] Department of Biology, College of Science and Humanities in Al-Kharj, Prince Sattam Bin Abdulaziz University, Al-Kharj 11942, Saudi Arabia

[2] Antibacterial Materials R&D Centre, China Metal New Materials (Huzhou) Institute, Huzhou, Zhejiang, China

[3] Department of Botany & Microbiology, College of Science, King Saud University, Riyadh 11451, Saudi Arabia

**Graphical Abstract**

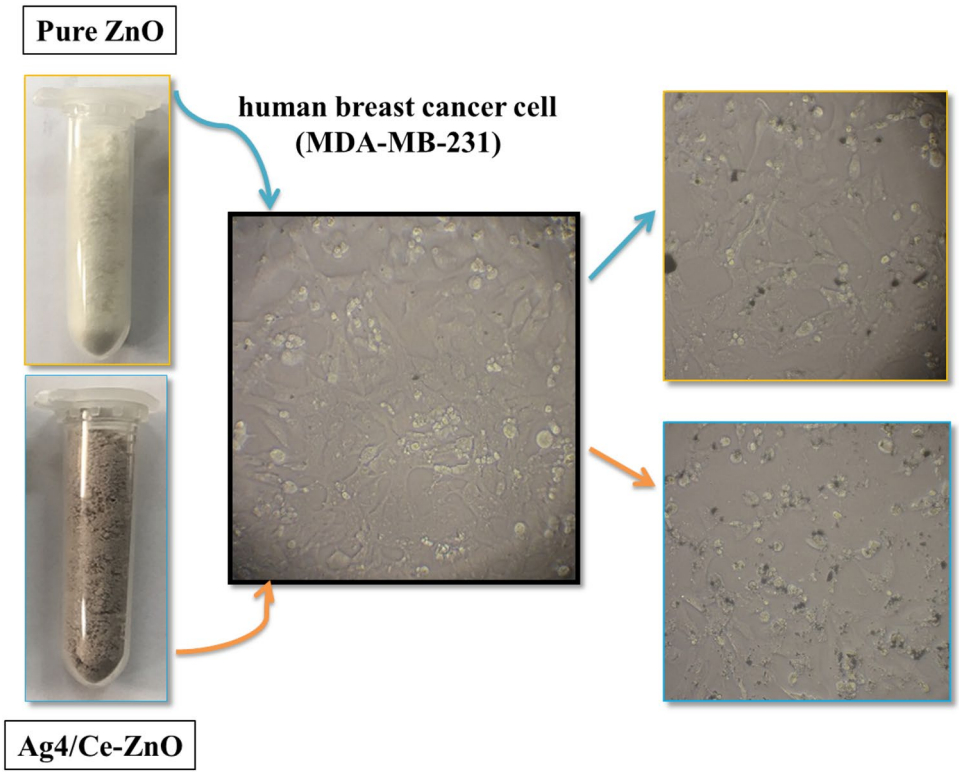


**Keywords** Ag and Ce dual-doped ZnO NPs · Green synthesis · MDA-MB-231 cells · MTT assay

## Introduction

As a novel type of widely used mineral particles [1], metal–organic framework [2] and metallic nanoparticles [3–5] such as zinc oxide were noticed and explored by researchers due to their suitable mechanical [6, 7], physical [8, 9] and chemical properties [10–13] that are combined with a higher adsorption power than other zinc-containing compounds [14, 15]. Zinc oxide is one of the compounds of zinc that was recognized as a safe substance by the US Department of Food and Drug Administration [16]. The properties of nanostructures led to their various applications such as anticancer [17, 18], tissue engineering [19–21], antimicrobial [22, 23], degradation [24], photocatalyst [25–29], antioxidant [30], sensor [31–36], sensing [37–39], agriculture [40–42], absorption [43], purification [44, 45], energy [46–49], anti-inflammatory therapy [50], food analysis [51], and drug carriers [52–54]. Among the notable properties of zinc oxide nanoparticles, one can point out their high chemical stability, low dielectric constant, high catalytic activity, absorption of infrared and ultraviolet light, and most importantly their antibacterial properties [55]. Confirming the therapeutic and toxic effects of these compounds can stand as a significant step throughout the advancements of cancer [56–63] and fungal/bacterial infection disease [64–66] treatments [67–69] such as COVID 19 [70, 71]. The primary prevention of infection [72–74] and cancers' diseases [75–77], new development in research [78–80] and innovation [81–84], such as nanotechnology [85, 86], materials [87–89] and digital technologies [90], have the need to improve our understanding of diseases [91–93] such as cancer [94–97]. In fact, recent developments [98] in all field of science [99–101] and technology [102–104] have impact on human health [105–108] and life [109–112].

Although the main action mechanism of nanoparticles remains unknown[113–115], yet the results of various studies on in in vivo and in vitro environments [116, 117] were indicative of their ability to produce reactive oxygen species (ROS) [118–120], which consequently points out their potent functionality in intracellular calcium concentration, activation of transcription factors, and alterations in cytokines [121–123]. The various approaches of ROS in damaging cells include DNA damage [124–126], interference with cellular signaling pathways, changes in gene transcription, etc. [127–129].

There are different physical [130], chemical [61, 131], and biological methods [132–137] for synthesizing nanostructures, while the exertion of each technique is dependent on the available conditions and purpose of the synthesis [138]. The most common synthesizing methods for the prepare of zinc oxide nanoparticles are observed in the form of sol–gel [139], microemulsion, mechanical–chemical process, direct solvent evaporation, hydrothermal, and spark deposition, which is selected depending on certain factors such as surface chemistry, size distribution, particle morphology, and particle reaction in solution [140]. Next to the advantages of these procedures, there are disadvantages as well since the involved substances are toxic and their usage in medical research is limited [141, 142]. In addition, some of the applied materials remain insoluble and can cause environmental pollution [143–146]. Therefore, in recent years, the application of biological or green methods was noticeably highlighted in order to overcome the disadvantages [147–151]. Green synthesis is defined as the exertion of biological organisms, such as microorganisms, for completing the synthesizing processes that are composed of different bacteria species, actinomycetes [152], algae, fungi, bacteria [153], and biomass [154] or plant extracts [155–159]. Green synthesizing techniques lack the hazardous aspects of physical and chemical methods, and on the other hand, they were confirmed to be environmentally friendly [160] and cost-effective [161] without requiring the usage of high pressure, high energy, high temperature, and toxic chemicals [162–165]. The application of plant extracts for the synthesis of nanoparticles may be a better option than other biological methods since it is suitable for conducting large-scale synthesis while being more cost-effective, as well as capable of accurately preserving the cellular environment [166–168].

*Alhagi persarum* is a shrub with thin, branched, and prickly stems with an average height of 50 cm. The leaves of this plant are small, oval, pointed, and simple that grows at intervals from the stems. This plant mainly grows in hot and deserted areas (deserts) of Iran, especially in southern regions. A sugary substance is secreted from the stems of this plant that is known as *taranjabin* in Iran, which turns into white, yellow, or brownish-yellow droplets upon being exposed to air. The chemical composition of *taranjabin* includes 47.7% of melezitose, 26.44% of sucrose, 11.64% of fructose reducing sugar, 12.4% of gum, and mucilage and 5.1% of ash. *Taranjabin* is recognized as a laxative that can relieve rheumatic, chest, cough, fever, and biliary pains, which is used in traditional medicine for the treatment of jaundice in infants, as well as children with rubella and infectious fevers.

In order to discover fast and effective treatment pathways or to produce materials with high therapeutic effects for the treatment of cancer, this study attempted to synthesize Ag and Ce dual-doped ZnO NPs by the usage of *taranjabin* for the very first time and evaluated the cytotoxic activity of synthesized nanoparticles on human breast cancer (MDA-MB-231) and breast normal (MCF-10A) cells lines. In addition, we investigated the antimicrobial activity against harmful bacteria.

## Materials and methods

### Synthesis of pure and dual-doped ZnO NPs

The synthesis of Ag and Ce dual-doped ZnO NPs was started with preparing the Ce:Ag ratios of 1:1, 1:2, and 1:4. Then, 0.3 gr of *taranjabin* was dissolved in 50 mL of distilled water within four Erlenmeyer flasks to arrange one sample of un-doped and three samples of dual-doped nanoparticles, respectively. In the following, subsequent to the addition of zinc nitrate hexahydrate (0.02 M, $Zn(NO_3)_2.6H_2O$, Merck) to all the four *taranjabin* solutions, silver nitrate ($AgNO_3$, Merck) and cerium nitrate hexahydrate ($Ce(NO_3)_3.6H_2O$, Merck) were appended in accordance with the specified ratios, respectively. Once the solutions were mixed by a heater stirrer at 70 °C for 3 h, they were dried in an oven at 80 °C for 24 h. The resulting raw material was calcined at 600 °C for 2 h. The un-doped and cerium and silver dual-doped ZnO NPs were labeled as ZnO, Ag1/Ce–ZnO, Ag2/Ce–ZnO, and Ag4/Ce–ZnO, respectively (Fig. 1).

### Characterization

The size, morphology, and other physical–chemical properties of synthesized nanoparticles were examined through the performance of PXRD (Netherlands, PANalyticalX'Pert PRO MPD system, Cu Kα), UV–Vis (Rayleigh: UV-2100, China), Raman spectra that were captured by a Raman Takram P50C0R10 device at the laser wavelength of 532 nm,

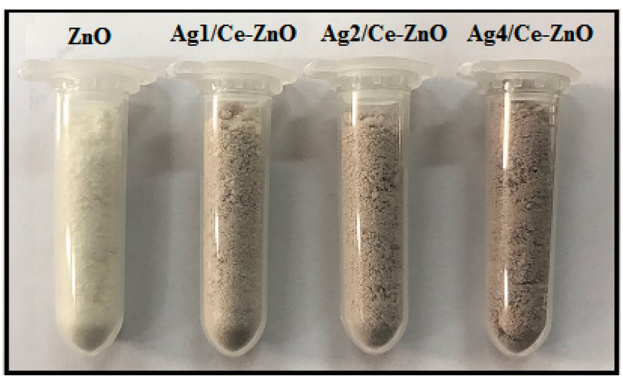


**Fig. 1** Images of biosynthesized pure ZnO, Ag1/Ce–ZnO, Ag2/Ce–ZnO, and Ag4/Ce–ZnO nanoparticles using *taranjabin*

FESEM (MIRA3 TESCAN, Czech), and UV–visible spectroscopy (UV–Vis, UV-1800, SHIMADZU) analyses.

## Cytotoxic

### Cells' culture

In this study, human breast cancer (MDA-MB-231) and breast normal (MCF-10A) cells were used to evaluate the cytotoxicity of synthesized nanoparticles. MCF-10A and MDA-MB-231 cells were obtained from the Pasteur Institute of Iran and thawed in prior to being cultured. The cells were transferred to Falcon tubes and centrifuged at 833 rpm for 9 min. Once the supernatant was removed, a complete culture medium was added to the cells to have the prepared suspensions poured into flasks. High-glucose DMEM culture medium was exerted for the process of cells culturing and the next step required the addition of 10% fetal bovine serum (FBS), 100 µg/mL of streptomycin, and 100 international units/mL of penicillin to each culture medium to prevent the inducement of microbial growth. In order to proliferate and grow the cells, the culture medium was incubated under 5% $CO_2$ at 37 °C.

### MTT assay

Human breast cancer (MDA-MB-231) and breast normal (MCF-10A) cells were cultured in an incubator with a high glucose DMEM that was supplemented with 10% fetal bovine serum and 1% penicillin/streptomycin solution (37 ◦C, 5% $CO_2$) until the cells count of each well of 96-well plate reached 10,000. The culture medium was replaced with 100 µL of the DMEM that contained the formulations at different concentrations (1, 10, 50, 100, and 500 µg/mL) to be seeded for another 24 h. Three duplications were considered for each concentration. In the following, the culture medium was changed after 24 h along with the replacement of fresh high glucose DMEM. Then, 20 µL of 5 mg/mL 3-(4, 5-dimethylthiazol-2-yl)-2, 5-diphenyl tetrazolium bromide (MTT) solution was added to each well and another course of incubation was performed for 4 h. Once 100 µL of DMSO was added to each well of 96-well plate, the resulting mixture was shaken for about 15 min at room temperature to dissolve the formazan. A microplate reader was exerted to measure the optical density (OD) at 570 nm. In addition, the cells viability rate (VR) was calculated according to the following equation:

$$VR = A/A_0 \times 100\%$$

in which A represents the absorbance of the cells that were treated with formulations and $A_0$ refers to the absorbance of control group.

### Antibacterial assay

The antibacterial test was studied on *Pseudomonas aeruginosa* using macrodilution method. The *P. aeruginosa* were cultured on these culture media in contact with nanoparticles. The concentrations of 1–250 mg/mL of nanoparticles were prepared in the Mueller Hinton culture medium. Then, the samples were placed in an incubator at 37 °C for 24 h. Finally, bacterial turbidity in the culture media was observed. The turbidity was a sign of the growth of the microbial strain in that concentration of nanoparticles.

### $IC_{50}$

The conduction of probit test was completed through the exertion of SPSS software for two purposes including the calculation of drug and nanoparticles concentrations that could limit the growth of 50% of cells ($IC_{50}$) and to measure the restriction percentage of cells growth against concentration.

## Results and discussion

### XRD analysis

Figure 2 presents the XRD pattern of biosynthesized pure ZnO, Ag1/Ce–ZnO, Ag2/Ce–ZnO, and Ag4/Ce–ZnO nanoparticles. The observed peaks in pure ZnO nanoparticles and Ag and Ce dual-doped ZnO nanoparticles were indexed to (100), (002), (101), (102), (110), (103), (200), (112), and (201), which is comparable with the hexagonal structure of ZnO (JCPDS-36–1451). In conformity to Fig. 2, increasing the ratio of Ag resulted in the appearance of peaks related to the silver-doped nanoparticles throughout the PXRD pattern. The purity and high crystalline form of synthesized nanoparticles was confirmed by the lack of observing any other additional peaks. The crystalline size of synthesized nanoparticles was calculated through the Debye–Scherer formula as given in the following equation:

$$D = K\lambda/\beta \cos\theta \quad (2)$$

where D refers to the crystallite size of nanoparticles, K represents the shape factor, λ is the wavelength of applied radiation, β would be full width at half maxima (FWHM) in radians, and θ stands for the diffraction angle. The average crystallite size of synthesized nanoparticles was estimated by considering the full width at half maxima (FWHM) of XRD peak (101) through the usage of Debye–Scherer formula, which was obtained to be 19.14, 19.73, 22.05, and 22.20 nm for ZnO, Ag1/Ce–ZnO, Ag2/Ce–ZnO, and Ag4/

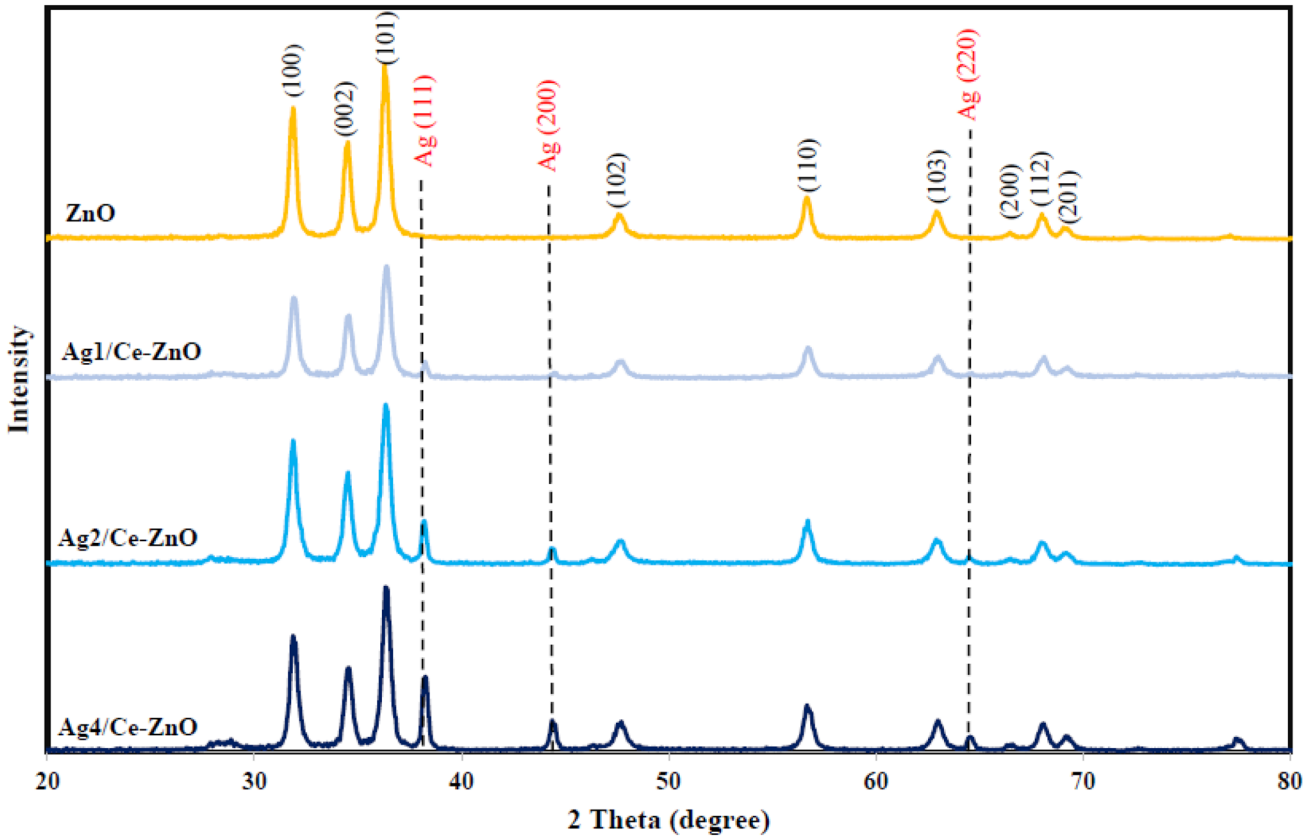


**Fig. 2** PXRD pattern of biosynthesized pure ZnO, Ag1/Ce–ZnO, Ag2/Ce–ZnO, and Ag4/Ce–ZnO nanoparticles using *taranjabin*

Ce–ZnO nanoparticles, respectively. The data in Fig. 2 indicate that the doping of Ce and Ag metals to the crystalline network of ZnO nanoparticles caused an increasing in the crystalline size of synthesized doped nanoparticles due to the difference in ionic radius of zinc atom (1.38 Å) when compared to silver (1.26 Å) and cerium (1.037 Å).

## FESEM and EDX analyses

Figure 3 presents the FESEM images of biosynthesized pure ZnO, Ag1/Ce–ZnO, Ag2/Ce–ZnO, and Ag4/Ce–ZnO nanoparticles obtained by the usage of *taranjabin*, which displays the approximately spherical shape of ZnO particles. The recorded doped nanoparticles throughout the FESEM images were also spherical, while observations indicated the inducement of an increasing in the size of synthesized particles due to the doping of Ag and Ce metals into the structure of ZnO. The mean particle size distribution of synthesized ZnO, Ag1/Ce–ZnO, Ag2/Ce–ZnO, and Ag4/Ce–ZnO nanoparticles, which were estimated to be 31.59, 31.93, 36.89, and 38.44 nm, exhibits the satisfying growth of particles as a result of increasing the percentage of doped metals. In conformity to the provided EDX profiles of biosynthesized ZnO and Ag4/Ce–ZnO nanoparticles in Fig. 4, the synthesized nanoparticles contained a high-purity content with the composition of Zn and O elements for ZnO and Zn, as well as O, Ag, and Ce elements for Ag4/Ce–ZnO nanoparticles. The table form of elemental composition is inserted in Fig. 4.

## Raman analysis

Raman spectroscopy is a non-destructive chemical analysis technique for providing detailed information about chemical structure, phase and polymorphy, crystallinity, and molecular interactions, which is based upon the interaction of light with chemical bonds within a material. According to group theory, ZnO nanoparticles contain a hexagonal wurtzite structure with a space group of P63mc. The optical modes of A1 + 2B2 + E1 + 2E2 imply the wurtzite structure of ZnO, which includes A1 + E1 + 2E2 as the active Raman mode, A1 + E1 as the active infrared mode, and 2B1 as the silent Raman mode. The A1 and E1 modes are two polar branches that are divided into longitudinal optical (LO) and transverse optical (TO). The A1, E1, and E2 modes are recognized as the first-order Raman active and based on Raman law, B1 modes are usually inactive throughout the Raman spectrum and are known as the silent modes. The Raman spectra of

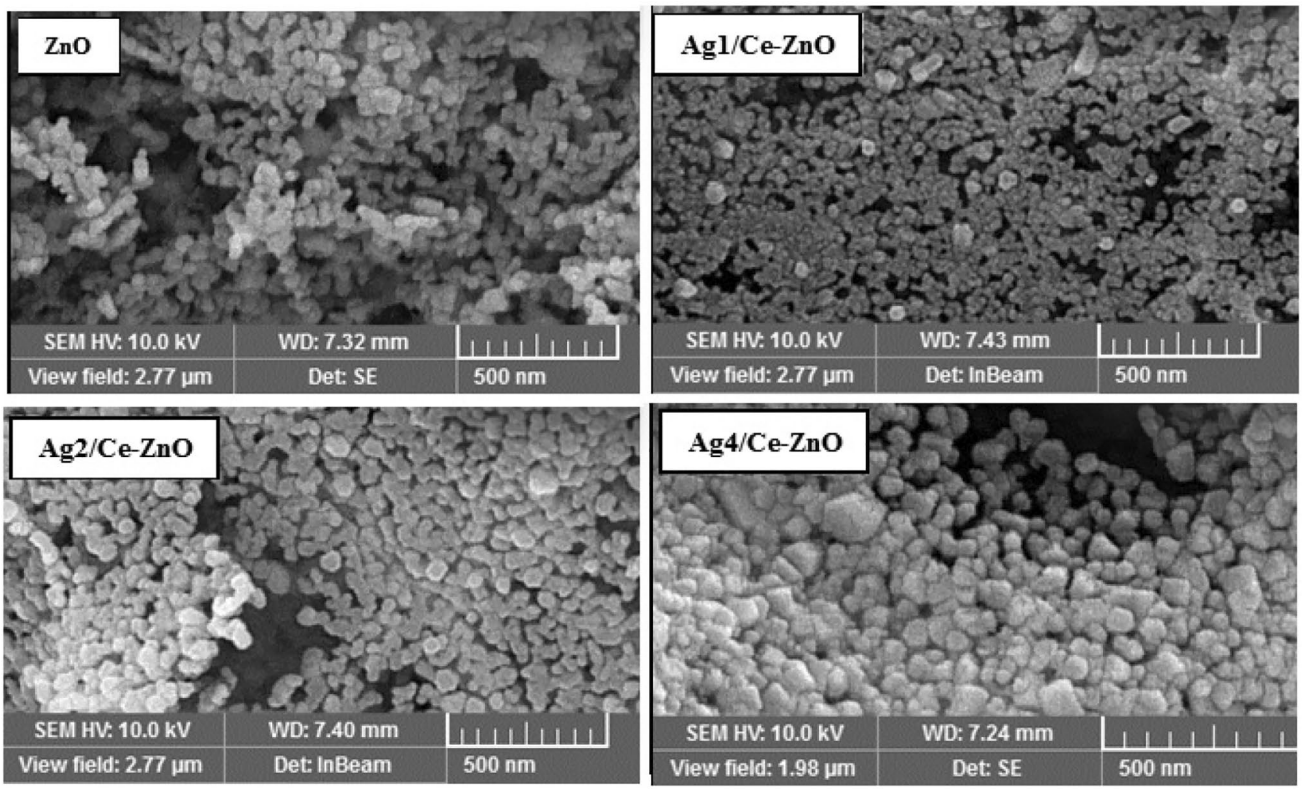


**Fig. 3** FESEM images and particle size distribution of biosynthesized pure ZnO, Ag1/Ce–ZnO, Ag2/Ce–ZnO, and Ag4/Ce–ZnO nanoparticles using *taranjabin*

biosynthesized pure ZnO, Ag1/Ce–ZnO, Ag2/Ce–ZnO, and Ag4/Ce–ZnO nanoparticles are represented in Fig. 5.

The main phonon states of ZnO nanoparticles with a hexagonal structure appeared in the regions of 583, 441, 345, 91 $cm^{-1}$, which were in correspondence to the A1(LO)–E1(LO), E2H, A1(TO), and E2H modes, respectively. The 2E2L mode was in correlation to the second-order phonon mode that appeared in the region of 132 $cm^{-1}$. Moreover, the modes of 3E2H-E2L, E1(TO) + E2L, 2(E2H-E2L), and A1(TO) + E1(TO) + E2L were related to the poly-phonon scattering that was detected in the points of 324, 475, 658, and 1105 $cm^{-1}$, respectively.

As it is displayed in Fig. 5, the doping factor (both Ag and Ce) of ZnO matrix caused significant changes in the polar and non-polar states. The E2H state involves the oxygen motion, while being sensitive to internal stress, and containing the characteristics of hexagonal structure of zinc oxide nanoparticles. Due to the decomposition of impurities and defects, the E2H mode faced a sharp decrease in the peak intensities of doped samples. In addition, this mode was observed to be steadily decreased and expanded as the doping concentrations of silver and cerium were increased. The detected polarity of A1(LO)–E1(LO) at around 583 $cm^{-1}$ was related to the doping of silver and cerium that can expand a peak and also force its shifting towards lower energies. All the variations and extensions of phonon modes were obtained by scattering contributions outside the center of Brillouin area. The phonon state of A1 (LO)–E1 (LO) is usually attributed to the interfacial defect of zinc and oxygen vacancy throughout the network of ZnO. Due to the combination of Ag and Ce ions with ZnO nanoparticles, the intensity of ZnO Raman peaks can be greatly increased through the doping of silver and cerium. In addition, further results confirmed the crystallization of ZnO nanoparticles with few defects due to the presence of Ag and Ce ions.

## UV–Vis analysis

Electron spectroscopy is a technique for investigating the energy distribution of ejected electrons from a material as a result of being irradiated by a source of ionizing irradiation. Figure 6 presents the electronic spectra of biosynthesized pure ZnO, Ag1/Ce–ZnO, Ag2/Ce–ZnO, and Ag4/Ce–ZnO nanoparticles obtained by the usage of *taranjabin*. The maximum wavelength of pure ZnO, Ag1/Ce–ZnO, Ag2/Ce–ZnO, and Ag4/Ce–ZnO nanoparticles were observed at the regions of 396, 372, 383, and 385 nm, respectively.

An increase in the concentration of Ce and Ag throughout the structure of ZnO causes a shifting in the absorption spectra towards higher wavelengths (red shift) due to the

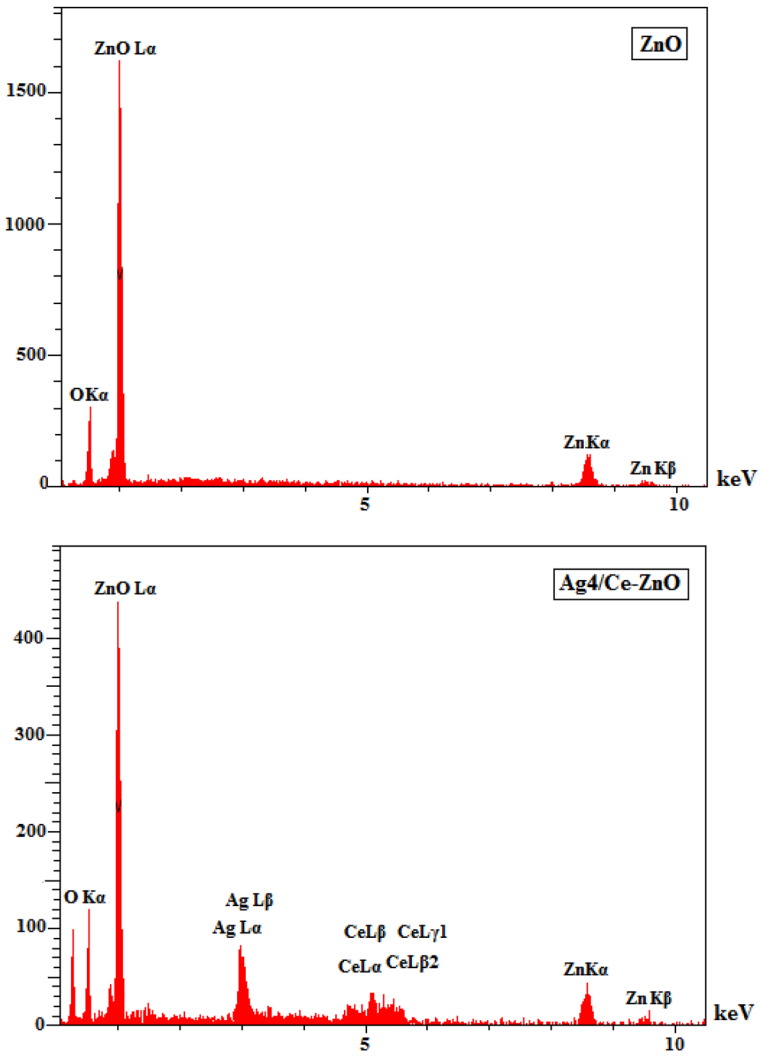


**Fig. 4** EDX profiles of biosynthesized pure ZnO and Ag4/Ce–ZnO nanoparticles using *taranjabin*

induced alteration in the amount of optical bandgap. This red shift represents the increasing crystallization and the effects of quantum confinement. An enlargement in the electron population during the doping of Ce and Ag into ZnO can lead to quantum constraints and finally cause a red shift in optical absorption behavior.

## Cytotoxic performance

In this study, we examined the cytotoxicity effects of biosynthesized ZnO, Ag1/Ce–ZnO, Ag2/Ce–ZnO, and Ag4/Ce–ZnO nanoparticles obtained by the usage of *taranjabin* against breast normal cells (MCF-10A) and breast cancer cells (MDA-MB-231). For this purpose, the cells were exposed for 24 h at different concentrations (1–500 µg/mL) of un-doped and dual-doped ZnO nanoparticles through the means of MTT assay (Fig. 7). In conformity to Fig. 6, the pure and Ag and Ce dual-doped ZnO nanoparticles did not cause any significant toxicity effects on the normal cell line (MCF-10A), while the doped nanoparticles resulted in almost similar toxicity impacts to that of un-doped nanoparticles. Furthermore, increasing the concentrations of doped and un-doped nanoparticles did not cause any significant toxicity effects. The assessment results of cytotoxic activity of synthesized nanoparticles on breast cancer cell line (MDA-MB-231) are presented in Fig. 7. According to observations, increasing the applied concentration intensified the effects of cytotoxicity, which reached a significant point at the concentration of 500 µg/mL. The cytotoxic effect of doped nanoparticles was more that of un-doped nanoparticles. As, 80% of the cells were killed from being treated with Ag4/Ce–ZnO nanoparticles at the concentration of 500 µg/mL. In addition, $IC_{50}$ data strongly confirmed the obtained results (Table 1), which less $IC_{50}$ was attributed to Ag4/Ce–ZnO nanoparticles. Hence, Ag4/Ce–ZnO nanoparticles show the greatest effect of toxicity. Figure 8 depicts the effect of synthesized nanoparticles being treated with breast normal cell and breast cancer cell lines. This figure clearly displays the difference in the cytotoxic activity of synthesized pure and dual-doped ZnO nanoparticles against these

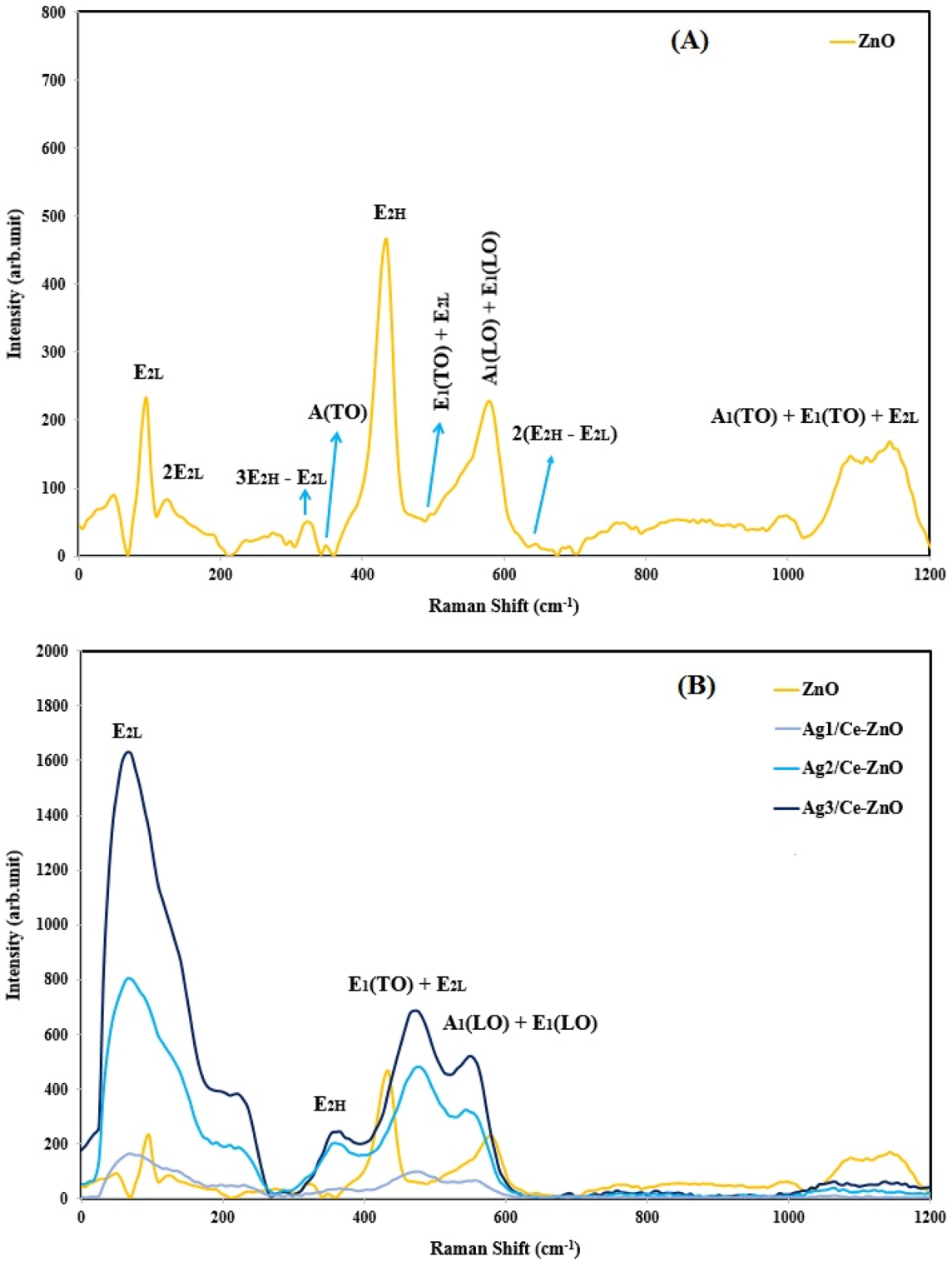


**Fig. 5** Raman spectra of biosynthesized (A) pure ZnO nanoparticles, and (B) ZnO, Ag1/Ce–ZnO, Ag2/Ce–ZnO, and Ag4/Ce–ZnO nanoparticles using *taranjabin*

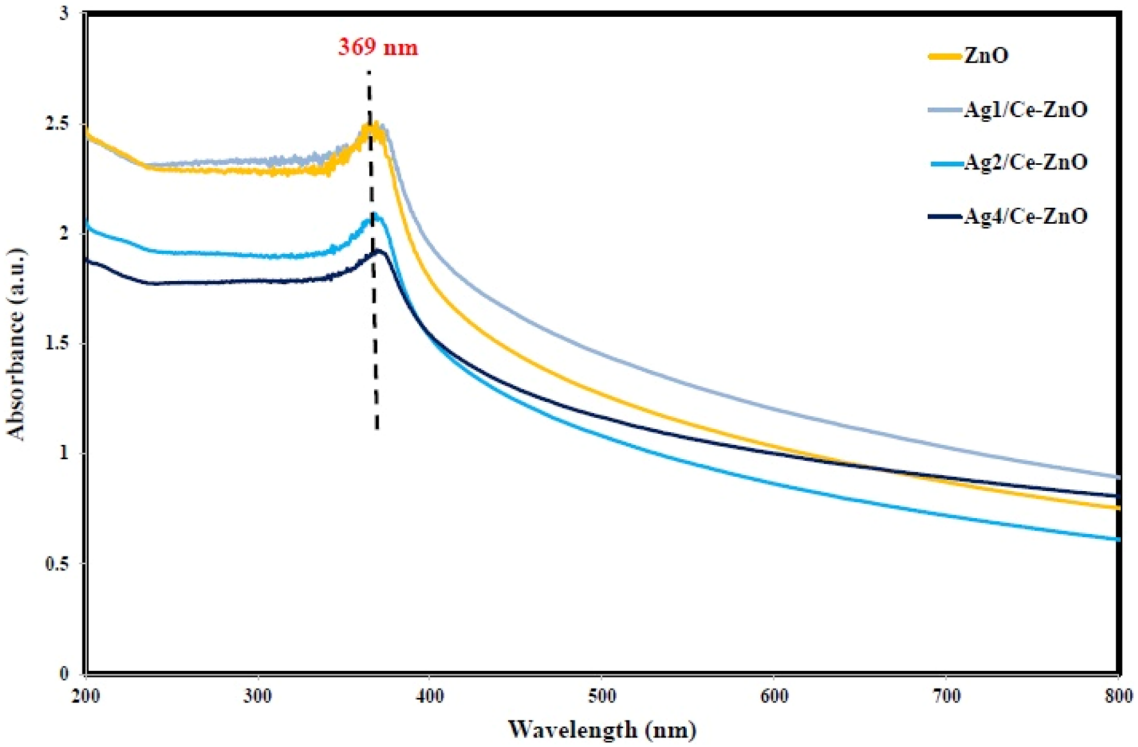


**Fig. 6** Electronic graph of biosynthesized pure ZnO, Ag1/Ce–ZnO, Ag2/Ce–ZnO, and Ag4/Ce–ZnO nanoparticles using *taranjabin*

two cell lines. These results suggested that the synthesized nanoparticles induced cytotoxicity in cancer cells without affecting the normal cells.

The cytotoxic effects of green synthesized doped ZnO NPs on cancer cells were mentioned in the work of many authors. For example, MJ Akhtar et al. studied the oxidative stress-mediated cytotoxicity of Al-doped ZnO nanoparticles against MCF-7 cells. According to their report, Al-doping was able to enhance the cytotoxicity and oxidative stress responses of ZnO nanoparticles against MCF-7 cells. In addition, they obtained an $IC_{50}$ of 44 µg/mL for un-doped ZnO nanoparticles and 31 µg/ml for the Al-doped ZnO counterparts. It was suggested by their results that Al-doped ZnO nanoparticles can induce apoptosis in MCF-7 cells through the mitochondrial pathway [169]. In another work, G. Vijayakumar et al. investigated the cells viability, ROS generation, and nanoparticle cells penetration rate of PEG encapsulated bare and Mn-doped ZnO nanoparticles against human liver carcinoma Huh7 cell lines. Based on their findings, un-doped the Mn-doped ZnO nanoparticles exhibited a higher cells annihilation effect, which may be due to the combined effects of $Zn^{2+}$ ion release and intracellular ROS generation; therefore, the inducement of apoptosis can be expected due to oxidative stress and ROS generation [170]. Considering these facts, doped metal oxide nanoparticles can stand as an attractive research topic for biomedical applications. Nano-sized materials have enabled many developments in biomedicine and other biological applications such as drug delivery, anticancer activity, gene delivery, fluorescent biological labels, protein detection, MRI contrast enhancement, probing of DNA, tissue engineering, phagokinetic studies, hyperthermia, and filtration of biological based molecular cell.

The antibacterial test of doped and non-doped nanoparticles was on *P. aeruginosa* and *E.coli*. The $IC_{50}$ was at 50 µg/mL.

## Conclusion

Un-doped and Ag and Ce dual-doped ZnO NPs were synthesized through a facile green method by exerting the extract of *taranjabin*. The obtained PXRD spectra displayed the hexagonal phase of un-doped and dual-doped ZnO NPs. SEM mapping demonstrated the homogeneous distribution of Ag and Ce in ZnO with high-quality lattice fringes while lacking any distortions. According to cytotoxicity results, the un-doped ZnO NPs displayed a similar toxicity effect on breast cancer cells (MDA-MB-231) to that of dual-doped ZnO NPs. Considering the comparable toxicity effect of

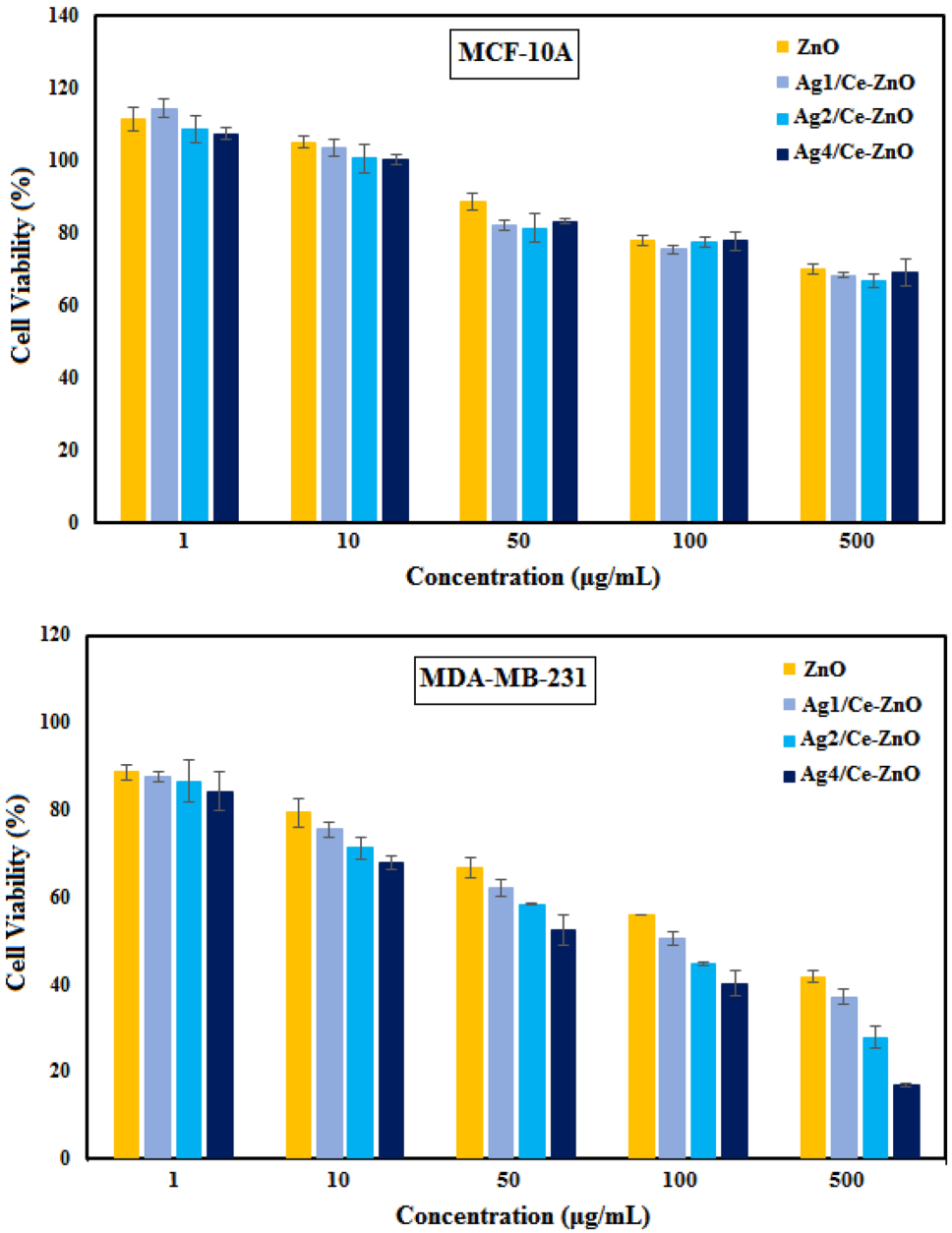


**Fig. 7** The cytotoxic activity of biosynthesized pure ZnO, Ag1/Ce–ZnO, Ag2/Ce–ZnO, and Ag4/Ce–ZnO nanoparticles using *taranjabin*

**Table 1** $IC_{50}$ values of biosynthesized pure ZnO, Ag1/Ce–ZnO, Ag2/Ce–ZnO, and Ag4/Ce–ZnO nanoparticles using *taranjabin*

| Cell lines | IC50 values (µg/mL) | | | |
|---|---|---|---|---|
| | ZnO | Ag1/Ce–ZnO | Ag2/Ce–ZnO | Ag4/Ce–ZnO |
| MCF-10A | 604.2647 | 799.8132 | 778.4796 | 878.4803 |
| MDA-MB-231 | 447.3 | 418.113 | 325.833 | 220.461 |

doped nanoparticles with the un-doped nanoparticles, it can be stated that the simultaneous doping of cerium and silver did cause significant alterations in the cytotoxic properties of zinc oxide nanoparticles. However, this discovery requires further investigation since it may affect certain physical and biological properties such as luminescence, UV absorption, or antibacterial features of zinc oxide nanoparticles. Therefore, this attempt can stand as a useful approach due to the cosmetic and even industrial applications of zinc oxide nanoparticles.

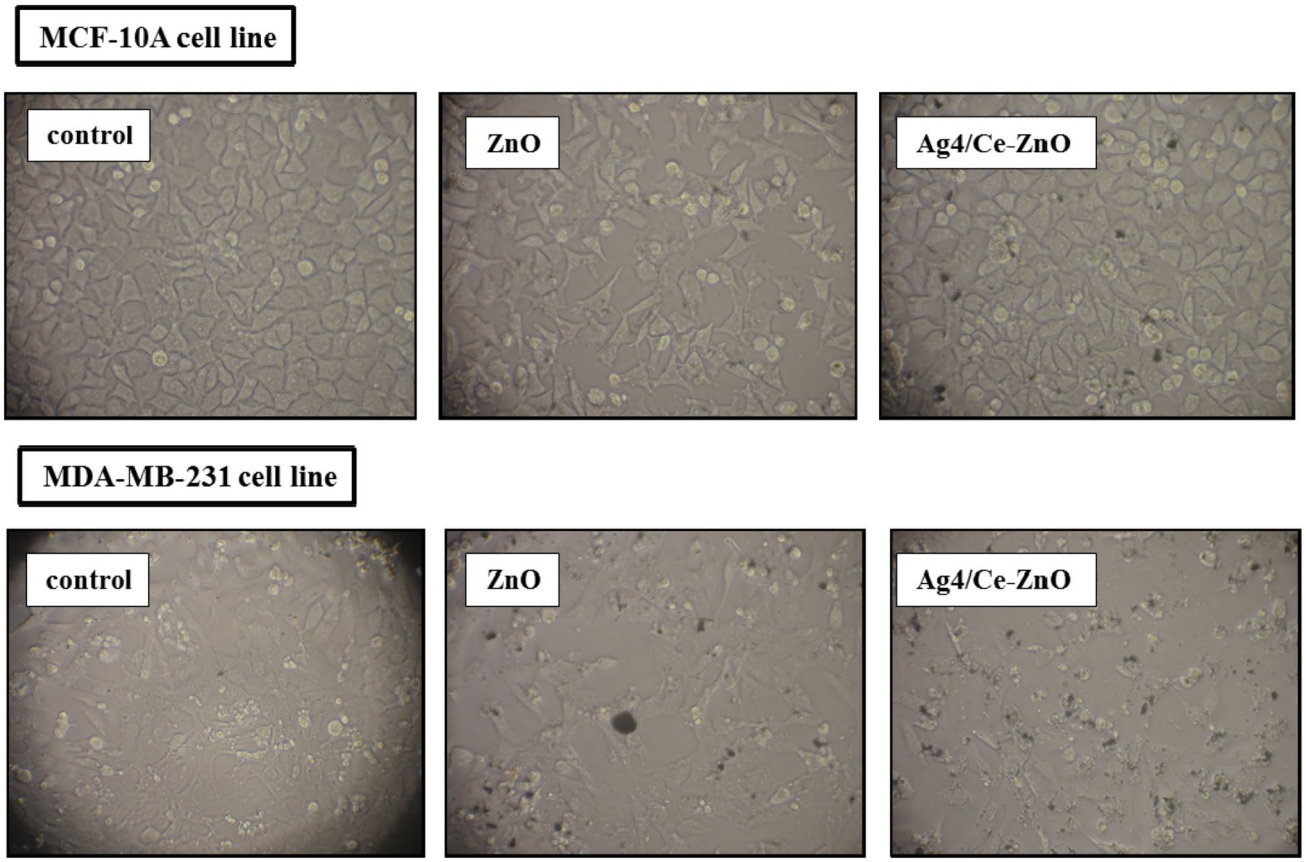


**Fig. 8** Images of breast normal cells (MCF-10A) and breast cancer cells (MDA-MB-231) lines treated with pure ZnO and Ag4/Ce–ZnO nanoparticles after 24 h treatment

**Acknowledgements** The authors extend their appreciation to the Deputyship for Research & Innovation, Ministry of Education in Saudi Arabia for funding this research work through the project number (IF2/PSAU/2022/01/22623).

## Declarations

**Conflict of interest** The authors confirm that the content of this article involves no competing interests.

## References

1. He X et al (2021) MgFe-LDH nanoparticles: a promising leukemia inhibitory factor replacement for self-renewal and pluripotency maintenance in cultured mouse embryonic stem cells. Advanced Science 8(9):2003535
2. Zeng Q et al (2020) Hyperpolarized Xe NMR signal advancement by metal-organic framework entrapment in aqueous solution. Proc Natl Acad Sci 117(30):17558–17563
3. Jasim SA et al (2022) Investigation of crotonaldehyde adsorption on pure and Pd-decorated GaN nanotubes: A density functional theory study. Solid State Commun 348:114741
4. Xia J, Majdi A, Toghraie D (2022) Molecular dynamics simulation of friction process in atomic structures with spherical nanoparticles. Solid State Commun 346:114717
5. Jia D et al (2014) Experimental verification of nanoparticle jet minimum quantity lubrication effectiveness in grinding. J Nanopart Res 16(12):2758
6. Yang Y et al (2022) Machinability of ultrasonic vibration assisted micro-grinding in biological bone using nanolubricant. Front Mech Eng. https://doi.org/10.1007/s11465-022-0717-z
7. Duan Z et al. (2022) *Mechanical behavior and Semiempirical force model of aerospace aluminum alloy milling using nano biological lubricant.* Front Mech Eng
8. Gao T et al (2021) Grindability of carbon fiber reinforced polymer using CNT biological lubricant. Sci Rep 11(1):22535
9. Duan Z et al (2021) Milling surface roughness for 7050 aluminum alloy cavity influenced by nozzle position of nanofluid minimum quantity lubrication. Chin J Aeronaut 34(6):33–53
10. Jeevanandam J et al (2018) Review on nanoparticles and nanostructured materials: history, sources, toxicity and regulations. Beilstein J Nanotechnol 9(1):1050–1074
11. Raya I et al (2022) Role of compositional changes on thermal, magnetic, and mechanical properties of Fe-PC-based amorphous alloys. Chin Phys B 31(1):016401
12. Chupradit S et al Use of organic and copper-based nanoparticles on the turbulator installment in a shell tube heat exchanger: a CFD-based simulation approach by using nanofluids. J Nanomater 2021. 2021.
13. Hu X et al (2022) The microchannel type effects on water-Fe3O4 nanofluid atomic behavior: Molecular dynamics approach. J Taiwan Inst Chem Eng 135:104396

14. Khatami M et al (2018) Rectangular shaped zinc oxide nanoparticles: Green synthesis by Stevia and its biomedical efficiency. Ceram Int 44(13):15596–15602
15. Miri A et al (2019) Zinc oxide nanoparticles: Biosynthesis, characterization, antifungal and cytotoxic activity. Mater Sci Eng C 104:109981
16. Indhira D et al (2022) Biomimetic facile synthesis of zinc oxide and copper oxide nanoparticles from Elaeagnus indica for enhanced photocatalytic activity. Environ Res 212:113323
17. Cao Y et al (2021) Green synthesis of bimetallic ZnO–CuO nanoparticles and their cytotoxicity properties. Sci Rep 11(1):1–8
18. Vidhya MS et al (2021) Anti-cancer applications of Zr Co, Ni-doped ZnO thin nanoplates. Mater Lett 283:128760
19. Xue X et al. Rational Design of Multifunctional CuS Nanoparticle-PEG Composite Soft Hydrogel-Coated 3D Hard Polycaprolactone Scaffolds for Efficient Bone Regeneration. Advanced Functional Materials. **n/a**(n/a): p. 2202470.
20. Liu J et al (2022) Electrospun strong, bioactive, and bioabsorbable silk fibroin/poly (L-lactic-acid) nanoyarns for constructing advanced nanotextile tissue scaffolds. Materials Today Bio 14:100243
21. Arkaban H et al (2022) Polyacrylic Acid Nanoplatforms: Antimicrobial, Tissue Engineering, and Cancer Theranostic Applications. Polymers 14(6):1259
22. Hachem K et al (2022) Adsorption of Pb (II) and Cd (II) by magnetic chitosan-salicylaldehyde Schiff base: Synthesis, characterization, thermal study and antibacterial activity. J Chin Chem Soc 69(3):512–521
23. Obaid RF et al (2022) Antibacterial activity, anti-adherence and anti-biofilm activities of plants extracts against Aggregatibacter actinomycetemcomitans: An in vitro study in Hilla City *Iraq*. Caspian J Environment Sci 20(2):367–372
24. Turki Jalil A et al (2021) CuO/ZrO2 nanocomposites: facile synthesis, characterization and photocatalytic degradation of tetracycline antibiotic. J Nanostruct 11(2):333–346
25. Ameen F, Dawoud T, AlNadhari S (2021) Ecofriendly and low-cost synthesis of ZnO nanoparticles from Acremonium potronii for the photocatalytic degradation of azo dyes. Environ Res 202:111700
26. Selvam K et al. (2022) Laccase production from Bacillus aestuarii KSK using Borassus flabellifer empty fruit bunch waste as a substrate and assessing their malachite green dye degradation. J Appl Microbiol.
27. Aljumaily MM et al (2022) Modification of Poly (vinylidene fluoride-co-hexafluoropropylene) Membranes with DES-Functionalized Carbon Nanospheres for Removal of Methyl Orange by Membrane Distillation. Water 14(9):1396
28. Jasim SA et al (2022) Nanomagnetic Salamo-based-Pd (0) Complex: an efficient heterogeneous catalyst for Suzuki-Miyaura and Heck cross-coupling reactions in aqueous medium. J Mol Struct 1261:132930
29. Al-Nayili A et al (2022) Formic acid dehydrogenation using noble-metal nanoheterogeneous catalysts: towards sustainable hydrogen-based energy. Catalysts 12(3):324
30. Gangalla R et al (2021) Optimization and characterization of exopolysaccharide produced by Bacillus aerophilus rk1 and its in vitro antioxidant activities. J King Saud Univ Sci 33(5):101470
31. Yumashev AV, et al. (2022) *Optical-based biosensor for detection of oncomarker CA 125, recent progress and current status.* Anal Biochem 114750.
32. Chupradit S, et al. (2022) Various types of electrochemical biosensors for leukemia detection and therapeutic approaches. Anal Biochem, 114736.
33. Jalil AT et al (2021) High-sensitivity biosensor based on glass resonance PhC cavities for detection of blood component and glucose concentration in human urine. Coatings 11(12):1555
34. Chupradit S et al (2021) Ultra-sensitive biosensor with simultaneous detection (of cancer and diabetes) and analysis of deformation effects on dielectric rods in optical microstructure. Coatings 11(12):1564
35. Kartika R et al (2022) Ca12O12 nanocluster as highly sensitive material for the detection of hazardous mustard gas: Density-functional theory. Inorg Chem Commun 137:109174
36. Olegovich Bokov D et al (2022) Ir-decorated gallium nitride nanotubes as a chemical sensor for recognition of mesalamine drug: a DFT study. Mol Simul 48(5):438–447
37. Khaki N et al (2022) Sensing of acetaminophen drug using Zn-doped boron nitride nanocones: a DFT inspection. Appl Biochem Biotechnol 194(6):2481–2491
38. Sun S et al (2023) Selection and identification of a novel ssDNA aptamer targeting human skeletal muscle. Bioactive Mater 20:166–178
39. Hou Q. et al. (2022) Role of Nutrient-sensing Receptor GPRC6A in Regulating Colonic Group 3 Innate Lymphoid Cells and Inflamed Mucosal Healing. J Crohn's and Colitis
40. Gao T et al (2019) Dispersing mechanism and tribological performance of vegetable oil-based CNT nanofluids with different surfactants. Tribol Int 131:51–63
41. Lei J et al (2022) Intestinal microbiota regulate certain meat quality parameters in chicken. Front Nutr 9:747705
42. Nazaripour E et al (2022) Ferromagnetic nickel (II) oxide (NiO) nanoparticles: biosynthesis, characterization and their antibacterial activities. Rendiconti Lincei Scienze Fisiche e Naturali 33(1):127–134
43. Sadeghi M et al (2022) Dichlorosilane adsorption on the Al, Ga, and Zn-doped fullerenes. Monatshefte für Chemie-Chemical Monthly 153:427–434
44. ANZUM R. et al. (2022) A review on separation and detection of copper, cadmium, and chromium in food based on cloud point extraction technology. Food Sci Technol 2022. **42**.
45. Wu X et al (2021) Circulating purification of cutting fluid: an overview. Int J Adv Manufact Technol 117(9):2565–2600
46. Sivaraman R. et al (2022) Evaluating the potential of graphene-like boron nitride as a promising cathode for Mg-ion batteries. J Electroanal Chem 116413.
47. Li B et al (2017) Heat transfer performance of MQL grinding with different nanofluids for Ni-based alloys using vegetable oil. J Clean Prod 154:1–11
48. Li B et al (2016) Grinding temperature and energy ratio coefficient in MQL grinding of high-temperature nickel-base alloy by using different vegetable oils as base oil. Chin J Aeronaut 29(4):1084–1095
49. Anqi AE et al (2022) Effect of combined air cooling and nano enhanced phase change materials on thermal management of lithium-ion batteries. J Energy Storage 52:104906
50. Xue X et al (2022) Neutrophil-erythrocyte hybrid membrane-coated hollow copper sulfide nanoparticles for targeted and photothermal/ anti-inflammatory therapy of osteoarthritis. Compos B Eng 237:109855
51. Ngafwan N et al (2021) Study on novel fluorescent carbon nanomaterials in food analysis. Food Sci Technol 42(37821):1–6
52. Jasim SA et al (2022) MXene/metal and polymer nanocomposites: preparation, properties, and applications. J Alloy Compound 61:80–115
53. Saleh RO et al (2022) Application of aluminum nitride nanotubes as a promising nanocarriers for anticancer drug 5-aminosalicylic acid in drug delivery system. J Mol Liq 352:118676
54. Zhuo Z et al (2020) A Loop-based and AGO-incorporated virtual screening model targeting AGO-Mediated miRNA–mRNA interactions for drug discovery to rescue bone phenotype in genetically modified mice. Adv Sci 7(13):1903451

55. Saravanan M et al (2018) Green synthesis of anisotropic zinc oxide nanoparticles with antibacterial and cytofriendly properties. Microb Pathog 115:57–63
56. Swathi S et al (2020) Cancer targeting potential of bioinspired chain like magnetite (Fe3O4) nanostructures. Curr Appl Phys 20(8):982–987
57. Isacfranklin M et al (2020) Single-phase Cr2O3 nanoparticles for biomedical applications. Ceram Int 46(12):19890–19895
58. Isacfranklin M et al (2020) Y2O3 nanorods for cytotoxicity evaluation. Ceram Int 46(12):20553–20557
59. Sonbol H et al (2021) Padina boryana mediated green synthesis of crystalline palladium nanoparticles as potential nanodrug against multidrug resistant bacteria and cancer cells. Sci Rep 11(1):1–19
60. Ameen F et al (2021) Anti-oxidant, anti-fungal and cytotoxic effects of silver nanoparticles synthesized using marine fungus Cladosporium halotolerans. Appl Nanosci 12:1–9
61. Iram S et al (2017) Gold nanoconjugates reinforce the potency of conjugated cisplatin and doxorubicin. Colloids Surf, B 160:254–264
62. Kumar V et al (2022) Evaluation of cytotoxicity and genotoxicity effects of refractory pollutants of untreated and biomethanated distillery effluent using Allium cepa. Environ Pollut 300:118975
63. Jalil AT et al (2021) Cancer stages and demographical study of HPV16 in gene L2 isolated from cervical cancer in Dhi-Qar province, Iraq. Appl Nanosci 12:1–7
64. Mostafa AA-F et al (2020) In vitro evaluation of antifungal activity of some agricultural fungicides against two saprolegnoid fungi infecting cultured fish. J King Saud Univer Sci 32(7):3091–3096
65. Widjaja G et al (2021) Humoral immune mechanisms involved in protective and pathological immunity during COVID-19. Hum Immunol 82(10):733–745
66. Jalil AT, et al (2021) Polymerase chain reaction technique for molecular detection of HPV16 infections among women with cervical cancer in Dhi-Qar Province. Materials Today: Proceedings.
67. Sarika K et al (2021) Antimicrobial and antifungal activity of soil actinomycetes isolated from coal mine sites. Saudi J Biol Sci 28(6):3553–3558
68. Saleh MM et al (2020) Evaluation of immunoglobulins, CD4/CD8 T lymphocyte ratio and interleukin-6 in COVID-19 patients. Turkish J Immunol 8(3):129–134
69. Akter F et al (2022) Cocos nucifera endocarp extract exhibits anti-diabetic and antilipidemic activities in diabetic rat model. Int J Sci Res Dental Med Sci 4(1):8–15
70. Kausikan SP et al (2022) The impact of COVID-19 on auditory and visual choice reaction time of non-hospitalized patients: an observational study. Int J Sci Res Dental Med Sci 4(1):21–25
71. Li H et al (2021) Damaged lung gas exchange function of discharged COVID-19 patients detected by hyperpolarized 129Xe MRI. Sci Adv 7(1):eabc8180
72. Jalil AT et al (2020) Viral hepatitis in Dhi-Qar Province: demographics and hematological characteristics of patients. Int J Pharmaceutical Res 12(1):2081–2087
73. Hanan ZK et al (2021) Detection of human genetic variation in VAC14 gene by ARMA-PCR technique and relation with typhoid fever infection in patients with gallbladder diseases in Thi-Qar province/Iraq. Mater Today Proc. https://doi.org/10.1016/j.matpr.2021.05.236
74. Sotelo Núñez N et al (2020) Evaluation the effect of micro-osteoperforation on the tooth movement rate and the level of pain on miniscrew-supported maxillary molar distalization: a systematic review and meta-analysis. Int J Sci Res Dental Med Sci 2(3):81–86
75. Marofi F et al (2021) CAR-NK cell in cancer immunotherapy A promising frontier. Cancer Sci 112(9):3427–3436
76. Gowhari Shabgah A et al (2021) Does CCL19 act as a double-edged sword in cancer development? Clin Exp Immunol 207(2):164–175
77. Yan J et al (2020) Chiral protein supraparticles for tumor suppression and synergistic immunotherapy: an enabling strategy for bioactive supramolecular chirality construction. Nano Lett 20(8):5844–5852
78. Moghadasi S et al (2021) A paradigm shift in cell-free approach: the emerging role of MSCs-derived exosomes in regenerative medicine. J Transl Med 19(1):1–21
79. Jalil AT et al (2022) HEMATOLOGICAL AND SEROLOGICAL PARAMETERS FOR DETECTION OF COVID-19. J Microbiol Biotechnol Food Sci 11(4):e4229
80. Widjaja G et al (2022) Effect of tomato consumption on inflammatory markers in health and disease status: A systematic review and meta-analysis of clinical trials. Clin Nutr ESPEN 50:93–100
81. Marofi F et al (2021) Novel CAR T therapy is a ray of hope in the treatment of seriously ill AML patients. Stem Cell Res Ther 12(1):465
82. Vakili-Samiani S et al (2021) Targeting Wee1 kinase as a therapeutic approach in Hematological Malignancies. DNA Repair 107:103203
83. Xu Y et al (2022) Prediction of COVID-19 manipulation by selective ACE inhibitory compounds of Potentilla reptant root: In silico study and ADMET profile. Arab J Chem 15(7):103942
84. Zou M et al (2022) Gut microbiota on admission as predictive biomarker for acute necrotizing pancreatitis. Front Immunol 13:988326
85. Zhang Y et al (2016) Experimental study on the effect of nanoparticle concentration on the lubricating property of nanofluids for MQL grinding of Ni-based alloy. J Mater Process Technol 232:100–115
86. Gao T et al (2020) Surface morphology assessment of CFRP transverse grinding using CNT nanofluid minimum quantity lubrication. J Clean Prod 277:123328
87. Wang Y et al (2018) Processing Characteristics of Vegetable Oil-based Nanofluid MQL for Grinding Different Workpiece Materials. Int J Precis Eng Manuf - Green Technol 5(2):327–339
88. Cui X et al (2022) Grindability of titanium alloy using cryogenic nanolubricant minimum quantity lubrication. J Manuf Process 80:273–286
89. Duan C et al (2022) Accelerate gas diffusion-weighted MRI for lung morphometry with deep learning. Eur Radiol 32(1):702–713
90. Liu Q, Peng H, Wang Z-A (2022) Convergence to nonlinear diffusion waves for a hyperbolic-parabolic chemotaxis system modelling vasculogenesis. J Differ Equ 314:251–286
91. Alimadadi H, Ashraf H, Nasrabadi N (2019) Dens invaginatus with palatal expansion and buccal sinus tract: a case report. Int J Sci Res Dent Med Sci 1(3):52–56
92. Volodymyr A, Sergii K, Kozyk O (2021) Evaluation of the effectiveness of mini-screw-facilitated micro-osteoperforation interventions on the treatment process in patients with orthodontic treatment: a systematic review and meta-analysis. Int J Sci Res Dent Med Sci 3(3):147–152
93. Endriani R et al (2022) Aerobic bacteria and antibiotic sensitivity on odontectomy wound in RSUD Arifin Achmad Riau. Int J Sci Res Dent Med Sci 4(1):26–32
94. Qu Y-Y et al (2020) Inactivation of the AMPK–GATA3–ECHS1 pathway induces fatty acid synthesis that promotes clear cell renal cell carcinoma growth. Can Res 80(2):319–333
95. Li Y et al (2019) APC/CCDH1 synchronizes ribose-5-phosphate levels and DNA synthesis to cell cycle progression. Nat Commun 10(1):1–16

96. Wang D, et al. (2018) Colonic lysine homocysteinylation induced by high-fat diet suppresses DNA damage repair. Cell Rep **25**(2): 398–412.e6.
97. Wang D et al (2017) Lower circulating folate induced by a fidgetin intronic variant is associated with reduced congenital heart disease susceptibility. Circulation 135(18):1733–1748
98. Ding W et al (2022) Metabolic engineering of threonine catabolism enables Saccharomyces cerevisiae to produce propionate under aerobic conditions. Biotechnol J 17(3):2100579
99. Assi LN et al (2021) Early properties of concrete with alkali-activated fly ash as partial cement replacement. Proc Ins Civ Eng Constr Mater 174(1):13–20
100. Rahbaran M et al (2021) Cloning and embryo splitting in mammalians: brief history, methods, and achievements. Stem Cells Int 2021:2347506
101. Zhang J, Lv J, Wang J (2022) The crystal structure of (E)-1-(4-aminophenyl)-3-(p-tolyl) prop-2-en-1-one, C16H15NO. Z für Krist-New Cryst Struct 237(3):385–387
102. Yang W et al (2022) Turning chiral peptides into a racemic supraparticle to induce the self-degradation of MDM2. J Adv Res 3:S2090-1232(22)00121-7
103. Liu P, Shi J, Wang Z-A (2013) Pattern formation of the attraction-repulsion Keller-Segel system. Discrete & Continuous Dynamical Systems-B 18(10):2597
104. Jin H-Y, Wang Z-A (2020) Global stabilization of the full attraction-repulsion Keller-Segel system. Discret Contin Dyn Syst 40(6):3509–3527
105. Abosaooda M et al (2021) Role of vitamin C in the protection of the gum and implants in the human body: theoretical and experimental studies. Int J Corros Scale Inhib 10(3):1213–1229
106. Widjaja G et al (2022) Mesenchymal stromal/stem cells and their exosomes application in the treatment of intervertebral disc disease: A promising frontier. Int Immunopharmacol 105:108537
107. Mahawar R et al (2022) Nasal cavity malignant solitary fibrous tumor: a case report. Int J Sci Res Dent Med Sci 4(1):42–44
108. Zheng J et al (2022) Visualization of Zika virus infection via a light-initiated bio-orthogonal cycloaddition labeling strategy. Front Bioeng Biotechnol 10:940511
109. Zhang X et al. (2022) Gestational Leucylation Suppresses Embryonic T-Box Transcription Factor 5 Signal and Causes Congenital Heart Disease. Adv Sci p. 2201034.
110. Cai K et al (2022) Nicotinamide mononucleotide alleviates cardiomyopathy phenotypes caused by short-chain enoyl-CoA hydratase 1 deficiency. Basic Translat Sci 7(4):348–362
111. Zhang X et al (2021) Homocysteine inhibits pro-insulin receptor cleavage and causes insulin resistance via protein cysteine-homocysteinylation. Cell Rep 37(2):109821
112. Xu S et al (2021) Ketogenic diets inhibit mitochondrial biogenesis and induce cardiac fibrosis. Signal Transduct Target Ther 6(1):1–13
113. Kim D-Y et al (2018) Green synthesis of silver nanoparticles using Laminaria japonica extract: Characterization and seedling growth assessment. J Clean Prod 172:2910–2918
114. Rao MP et al (2018) Synthesis of N-doped potassium tantalate perovskite material for environmental applications. J Solid State Chem 258:647–655
115. Mohanta YK et al (2018) Bio-inspired synthesis of silver nanoparticles from leaf extracts of Cleistanthus collinus (Roxb.): its potential antibacterial and anticancer activities. IET Nanobiotechnol 12:343–348
116. Megarajan S et al (2022) Synthesis of N-myristoyltaurine stabilized gold and silver nanoparticles: assessment of their catalytic activity, antimicrobial effectiveness and toxicity in zebrafish. Environ Res 212:113159
117. Subramaniyan SB et al (2022) Phytolectin-cationic lipid complex revive ciprofloxacin efficacy against multi-drug resistant uropathogenic Escherichia coli. Colloids Surf, A 647:128970
118. Mythili R et al (2018) Utilization of market vegetable waste for silver nanoparticle synthesis and its antibacterial activity. Mater Lett 225:101–104
119. Ameen F et al (2020) Soil bacteria Cupriavidus sp. mediates the extracellular synthesis of antibacterial silver nanoparticles. J Mol Struct 1202:127233
120. Salahdin OD et al (2022) Oxygen reduction reaction on metal-doped nanotubes and nanocages for fuel cells. Ionics 28:3409–3419
121. Khan A et al (2020) Fabrication and antibacterial activity of nanoenhanced conjugate of silver (I) oxide with graphene oxide. Mater Today Commun 25:101667
122. Begum I et al (2021) Facile fabrication of malonic acid capped silver nanoparticles and their antibacterial activity. J King Saud Univ Sci 33(1):101231
123. Sonbol H et al (2021) Bioinspired synthesize of CuO nanoparticles using *Cylindrospermum stagnale* for antibacterial, anticancer and larvicidal applications. Appl Nanosci 12:1–11
124. Rajadurai UM et al (2021) Assessment of behavioral changes and antitumor effects of silver nanoparticles synthesized using diosgenin in mice model. J Drug Delivery Sci Technol 66:102766
125. Ameen F et al (2022) Antioxidant, antibacterial and anticancer efficacy of Alternaria chlamydospora-mediated gold nanoparticles. Appl Nanosci 12:1–8
126. Tang W et al (2017) Tumor origin detection with tissue-specific miRNA and DNA methylation markers. Bioinformatics 34(3):398–406
127. Ameen F et al (2018) Flavonoid dihydromyricetin-mediated silver nanoparticles as potential nanomedicine for biomedical treatment of infections caused by opportunistic fungal pathogens. Res Chem Intermed 44(9):5063–5073
128. AlYahya S et al (2018) Size dependent magnetic and antibacterial properties of solvothermally synthesized cuprous oxide (Cu2O) nanocubes. J Mater Sci: Mater Electron 29(20):17622–17629
129. Khosravikia M et al (2022) A simulation study of an applied approach to enhance drug recovery through electromembrane extraction. J Mol Liq 15:119210
130. Naveenraj S et al (2018) A general microwave synthesis of metal (Ni, Cu, Zn) selenide nanoparticles and their competitive interaction with human serum albumin. New J Chem 42(8):5759–5766
131. Jasni MJF et al (2017) Fabrication, characterization and application of laccase–nylon 6,6/Fe3+ composite nanofibrous membrane for 3,3′-dimethoxybenzidine detoxification. Bioprocess Biosyst Eng 40(2):191–200
132. AlNadhari S et al (2021) A review on biogenic synthesis of metal nanoparticles using marine algae and its applications. Environ Res 194:110672
133. Wang K et al (2022) Upgrading wood biorefinery: an integration strategy for sugar production and reactive lignin preparation. Indust Crop Prod 187(1):115366–115368
134. Valarmathi N et al (2020) Utilization of marine seaweed Spyridia filamentosa for silver nanoparticles synthesis and its clinical applications. Mater Lett 263:127244
135. Ahmed B et al (2020) Destruction of cell topography, morphology, membrane, inhibition of respiration, biofilm formation, and bioactive molecule production by nanoparticles of Ag, ZnO, CuO, TiO2, and Al2O3 toward beneficial soil bacteria. ACS Omega 5(14):7861–7876
136. Alsamhary K et al (2020) Gold nanoparticles synthesised by flavonoid tricetin as a potential antibacterial nanomedicine to treat respiratory infections causing opportunistic bacterial pathogens. Microb Pathog 139:103928

137. Mythili R et al (2018) Biogenic synthesis, characterization and antibacterial activity of gold nanoparticles synthesised from vegetable waste. J Mol Liq 262:318–321
138. Hajimiri M et al (2022) Rational design, synthesis, *in vitro*, and *in silico* studies of chlorophenylquinazolin-4(3*H*)-one containing different aryl acetohydrazides as tyrosinase inhibitors. Chem Biodivers 19(7):e202100964
139. Bokov D et al (2021) Nanomaterial by sol-gel method: synthesis and application. Adv Mater Sci Eng 2021:5102014
140. Cao Y et al (2022) Ceramic magnetic ferrite nanoribbons: Eco-friendly synthesis and their antifungal and parasiticidal activity. Ceram Int 48(3):3448–3454
141. Guo S et al (2017) Experimental evaluation of the lubrication performance of mixtures of castor oil with other vegetable oils in MQL grinding of nickel-based alloy. J Clean Prod 140:1060–1076
142. Sadeghi H et al (2022) Iron oxyhydroxide nanoparticles: green synthesis and their cytotoxicity activity against A549 human lung adenocarcinoma cells. Rendiconti Lincei Scienze Fisiche e Naturali 33(2):461–469
143. Awad ES et al (2022) Groundwater Hydrogeochemical and Quality Appraisal for Agriculture Irrigation in Greenbelt Area, Iraq. Environments 9(4):43
144. Fitriyah A et al (2022) Exposure to ambient air pollution and osteoarthritis; an animal study. Chemosphere 301:134698
145. Sarjito ME et al (2021) CFD-based simulation to reduce greenhouse gas emissions from industrial plants. Int J Chem Reactor Eng 19(11):1179–1186
146. Zhang J et al (2018) Experimental assessment of an environmentally friendly grinding process using nanofluid minimum quantity lubrication with cryogenic air. J Clean Prod 193:236–248
147. Moghadam NCZ et al (2022) Nickel oxide nanoparticles synthesis using plant extract and evaluation of their antibacterial effects on Streptococcus mutans. Bioprocess Biosyst Eng 45(7):1201–1210
148. Xie Y (2022) A multiscale biomimetic strategy to design strong, tough hydrogels by tuning the self-assembly behavior of cellulose. J Mat Chem A 10(45):1–6
149. Al-Enazi NM et al (2021) Tin oxide nanoparticles (SnO2-NPs) synthesis using *Galaxaura elongata* and its anti-microbial and cytotoxicity study: a greenery approach. Appl Nanosci 12:1–9
150. Rahim M et al (2018) Nutratherapeutics approach against cancer: tomato-mediated synthesised gold nanoparticles. IET Nanobiotechnol 12(1):1–5
151. Ghodake SG et al (2018) Colorimetric detection of Cu2+ based on the formation of peptide–copper complexes on silver nanoparticle surfaces. Beilstein J Nanotechnol 9:1414–1422
152. Soltani Nejad M, Khatami M, Shahidi Bonjar GH (2016) Extracellular synthesis gold nanotriangles using biomass of Streptomyces microflavus. IET nanobiotechnol **10**(1):33–38
153. Mortazavi SM, et al. (2017) Bacterial biosynthesis of gold nanoparticles using Salmonella enterica subsp. enterica serovar Typhi isolated from blood and stool specimens of patients. J Cluster Sci. **28**(5): 2997–3007.
154. Alshehrei F, Al-Enazi NM, Ameen F (2021) Vermicomposting amended with microalgal biomass and biochar produce phytopathogen-resistant seedbeds for vegetables. Biomass Convers Biorefinery 13:1–8
155. Ghaffar S et al (2022) What is the influence of grape products on liver enzymes? A systematic review and meta-analysis of randomized controlled trials. Complement Ther Med 69:102845
156. Rudiansyah M et al (2022) Beneficial alterations in growth performance, blood biochemicals, immune responses, and antioxidant capacity of common carp (Cyprinus carpio) fed a blend of Thymus vulgaris, Origanum majorana, and Satureja hortensis extracts. Aquaculture 555:738254
157. Hou S et al (2022) Understanding of promoting enzymatic hydrolysis of combined hydrothermal and deep eutectic solvent pretreated poplars by Tween 80. Biores Technol 362(1):127825
158. Khatami M, Iravani S (2021) Green and eco-friendly synthesis of nanophotocatalysts: an overview. Comments Inorg Chem 41(3):133–187
159. Haghighat M et al (2022) Cytotoxicity properties of plant-mediated synthesized K-doped ZnO nanostructures. Bioprocess Biosyst Eng 45(1):97–105
160. Jasim SA et al (2022) Green synthesis of spinel copper ferrite (CuFe2O4) nanoparticles and their toxicity. Nanotechnol Rev 11(1):2483–2492
161. Akbarizadeh MR et al (2022) Cytotoxic activity and Magnetic Behavior of green synthesized iron oxide nanoparticles on brain glioblastoma cells. Nanomed Res J 7(1):99–106
162. Almansob A et al (2022) Effective treatment of resistant opportunistic fungi associated with immuno-compromised individuals using silver biosynthesized nanoparticles. Appl Nanosci 12:1–12
163. Mohammed AE et al (2022) In-silico predicting as a tool to develop plant-based biomedicines and nanoparticles: Lycium shawii metabolites. Biomed Pharmacother 150:113008
164. Begum I et al (2022) A combinatorial approach towards antibacterial and antioxidant activity using tartaric acid capped silver nanoparticles. Processes 10(4):716
165. Satarzadeh N (2022) Facile microwave-assisted biosynthesis of arsenic nanoparticles and evaluation their antioxidant properties and cytotoxic effects: a preliminary in vitro study. J Clust Sci 33(1):1
166. Mortezagholi B et al (2022) Plant-mediated synthesis of silver-doped zinc oxide nanoparticles and evaluation of their antimicrobial activity against bacteria cause tooth decay. Microsc Res Tech 85(11):3553–3564
167. Sabouri Z et al (2022) Plant-based synthesis of cerium oxide nanoparticles using Rheum turkestanicum extract and evaluation of their cytotoxicity and photocatalytic properties. Mater Technol 37(8):555–568
168. Akbarizadeh MR, Sarani M, Darijani S (2022) Study of antibacterial performance of biosynthesized pure and Ag-doped ZnO nanoparticles. Rendiconti Lincei. Scienze Fisiche e Naturali 33:613–621
169. Akhtar MJ et al (2015) Aluminum doping tunes band gap energy level as well as oxidative stress-mediated cytotoxicity of ZnO nanoparticles in MCF-7 cells. Sci Rep 5(1):1–16
170. Vijayakumar G, Boopathi G, Elango M (2019) In vitro cytotoxic efficacy of PEG encapsulated manganese-doped zinc oxide nanoparticles on hepatocellular carcinoma cells. Mater Technol 34(13):807–817